The Astronomical Journal, 160:129 (10pp), 2020 September https://doi.org/10.3847/1538-3881/aba835
© 2020. The American Astronomical Society. All rights reserved.

Transits of Known Planets Orbiting a Naked-eye Star

Stephen R. Kane[1], Selçuk Yalçınkaya[2], Hugh P. Osborn[3,4,5], Paul A. Dalba[1,33], Louise D. Nielsen[6], Andrew Vanderburg[7,34], Teo Močnik[1], Natalie R. Hinkel[8], Colby Ostberg[1], Ekrem Murat Esmer[9], Stéphane Udry[6], Tara Fetherolf[1], Özgür Baştürk[9], George R. Ricker[4], Roland Vanderspek[4], David W. Latham[10], Sara Seager[4,11,12], Joshua N. Winn[13], Jon M. Jenkins[14], Romain Allart[6], Jeremy Bailey[15], Jacob L. Bean[16], Francois Bouchy[6], R. Paul Butler[17], Tiago L. Campante[18,19], Brad D. Carter[20], Tansu Daylan[4,35], Magali Deleuil[3], Rodrigo F. Diaz[21], Xavier Dumusque[6], David Ehrenreich[6], Jonathan Horner[20], Andrew W. Howard[22], Howard Isaacson[20,23], Hugh R. A. Jones[24], Martti H. Kristiansen[25,26], Christophe Lovis[6], Geoffrey W. Marcy[23], Maxime Marmier[6], Simon J. O'Toole[27,28], Francesco Pepe[6], Darin Ragozzine[29], Damien Ségransan[6], C. G. Tinney[30], Margaret C. Turnbull[31], Robert A. Wittenmyer[20], Duncan J. Wright[20], and Jason T. Wright[32]

[1] Department of Earth and Planetary Sciences, University of California, Riverside, CA 92521, USA; skane@ucr.edu
[2] Ankara University, Graduate School of Natural and Applied Sciences, Department of Astronomy and Space Sciences, Tandogan, TR-06100, Turkey
[3] Aix-Marseille Université, CNRS, CNES, Laboratoire d'Astrophysique de Marseille, France
[4] Department of Physics and Kavli Institute for Astrophysics and Space Research, Massachusetts Institute of Technology, Cambridge, MA 02139, USA
[5] NCCR/PlanetS, Centre for Space & Habitability, University of Bern, Bern, Switzerland
[6] Observatoire de Genève, Université de Genève, 51 ch. des Maillettes, 1290 Sauverny, Switzerland
[7] Department of Astronomy, The University of Texas at Austin, Austin, TX 78712, USA
[8] Southwest Research Institute, 6220 Culebra Rd, San Antonio, TX 78238, USA
[9] Ankara University, Faculty of Science, Department of Astronomy and Space Sciences, Tandogan, TR-06100, Turkey
[10] Center for Astrophysics | Harvard & Smithsonian, 60 Garden Street, Cambridge, MA 02138, USA
[11] Department of Earth, Atmospheric and Planetary Sciences, Massachusetts Institute of Technology, Cambridge, MA 02139, USA
[12] Department of Aeronautics and Astronautics, MIT, 77 Massachusetts Avenue, Cambridge, MA 02139, USA
[13] Department of Astrophysical Sciences, Princeton University, 4 Ivy Lane, Princeton, NJ 08544, USA
[14] NASA Ames Research Center, Moffett Field, CA, 94035, USA
[15] School of Physics, University of New South Wales, Sydney, NSW 2052, Australia
[16] Department of Astronomy & Astrophysics, University of Chicago, 5640 South Ellis Avenue, Chicago, IL 60637, USA
[17] Earth & Planets Laboratory, Carnegie Institution of Washington, NW, Washington, DC, 20015-1305, USA
[18] Instituto de Astrofísica e Ciências do Espaço, Universidade do Porto, Rua das Estrelas, 4150-762 Porto, Portugal
[19] Departamento de Física e Astronomia, Faculdade de Ciências da Universidade do Porto, Rua do Campo Alegre, s/n, 4169-007 Porto, Portugal
[20] Centre for Astrophysics, University of Southern Queensland, Toowoomba, QLD 4350, Australia
[21] International Center for Advanced Studies (ICAS) and ICIFI (CONICET), ECyT-UNSAM, Campus Miguelete, 25 de Mayo y Francia (1650), Buenos Aires, Argentina
[22] Department of Astronomy, California Institute of Technology, Pasadena, CA 91125, USA
[23] Department of Astronomy, University of California, Berkeley, CA 94720, USA
[24] Centre for Astrophysics Research, University of Hertfordshire, Hatfield, Herts AL10 9AB, UK
[25] Brorfelde Observatory, Observator Gyldenkernes Vej 7, DK-4340 Tølløse, Denmark
[26] DTU Space, National Space Institute, Technical University of Denmark, Elektrovej 327, DK-2800 Lyngby, Denmark
[27] Australian Astronomical Observatory, North Ryde, NSW 2113, Australia
[28] Australian Astronomical Optics, Faculty of Science and Engineering, Macquarie University, North Ryde, NSW 2113, Australia
[29] Department of Physics and Astronomy, N283 ESC, Brigham Young University, Provo, UT 84602, USA
[30] Exoplanetary Science at USNW, School of Physics, UNSW Sydney, Sydney 2052, Australia
[31] SETI Institute, Carl Sagan Center for the Study of Life in the Universe, Off-Site: 2613 Waunona Way, Madison, WI 53713, USA
[32] Department of Astronomy & Astrophysics and Center for Exoplanets and Habitable Worlds and Penn State Extraterrestrial Intelligence Center, 525 Davey Laboratory, The Pennsylvania State University, University Park, PA 16802, USA
Received 2020 June 24; revised 2020 July 20; accepted 2020 July 20; published 2020 August 21

Abstract

Some of the most scientifically valuable transiting planets are those that were already known from radial velocity (RV) surveys. This is primarily because their orbits are well characterized and they preferentially orbit bright stars that are the targets of RV surveys. The Transiting Exoplanet Survey Satellite (TESS) provides an opportunity to survey most of the known exoplanet systems in a systematic fashion to detect possible transits of their planets. HD 136352 (Nu^2 Lupi) is a naked-eye ($V = 5.78$) G-type main-sequence star that was discovered to host three planets with orbital periods of 11.6, 27.6, and 108.1 days via RV monitoring with the High Accuracy Radial velocity Planet Searcher (HARPS) spectrograph. We present the detection and characterization of transits for the two inner planets of the HD 136352 system, revealing radii of $1.482^{+0.058}_{-0.056}\ R_\oplus$ and $2.608^{+0.078}_{-0.077}\ R_\oplus$ for planets b and c, respectively. We combine new HARPS observations with RV data from the Keck/High Resolution Echelle Spectrometer and the Anglo-Australian Telescope, along with TESS photometry from Sector 12, to perform a complete analysis of the system parameters. The combined data analysis results in extracted bulk density values of $\rho_b = 7.8^{+1.2}_{-1.1}$ g cm^{-3} and $\rho_c = 3.50^{+0.41}_{-0.36}$ g cm^{-3} for planets b and c, respectively, thus placing them on either side of the radius valley. The combination of the multitransiting planet system, the bright host star, and the diversity of

[33] NSF Astronomy and Astrophysics Postdoctoral Fellow.
[34] NASA Sagan Fellow.
[35] Kavli Fellow.

planetary interiors and atmospheres means this will likely become a cornerstone system for atmospheric and orbital characterization of small worlds.

Unified Astronomy Thesaurus concepts: Exoplanets (498); Exoplanet atmospheres (487); Exoplanet structure (495); Transit photometry (1709); Radial velocity (1332)

Supporting material: machine-readable table

1. Introduction

The discovery of transiting exoplanets has enabled a plethora of science not accessible through other exoplanet detection techniques. Transiting planets orbiting bright stars are especially important in furthering our knowledge of planetary systems because they offer unique windows into comparative exoplanetology. First, they allow for a measurement of both the planetary mass and radius, and thereby to place constraints on the planet interior structure. Second, they are amenable to atmospheric characterization through transmission spectroscopy (e.g., Sing et al. 2016; Kempton et al. 2018), to secondary eclipse measurements (e.g., Kreidberg et al. 2019), and to orbital geometry characterization through the Rossiter–McLaughlin effect (e.g., Fabrycky & Winn 2009). In multi-planet systems, they also allow for a deepened understanding of the system architecture through planet–planet dynamics accessible through the modeling of transit timing variations (e.g., Jontof-Hutter et al. 2016).

The Transit Ephemeris Refinement and Monitoring Survey (TERMS) has been operating since 2008 with the primary goal of detecting transits for known radial velocity (RV) exoplanets (Kane et al. 2009). The appeal of transits for known RV planets is that their orbits are already characterized and their host stars are relatively bright. Well-known examples of RV planets later found to transit include HD 209458b (Charbonneau et al. 2000; Henry et al. 2000), HD 189733b (Bouchy et al. 2005), and HD 80606b (Naef et al. 2001; Fossey et al. 2009; Garcia-Melendo & McCullough 2009; Laughlin et al. 2009). Though the TERMS survey successfully discovered new planets (Wang et al. 2012), destroyed old planets (Kane et al. 2016b), characterized numerous host stars (e.g., Dragomir et al. 2012; Hinkel et al. 2015), and ruled out transits (e.g., Kane et al. 2011a, 2011b; Pilyavsky et al. 2011; Henry et al. 2013), the primary science goal was largely impeded by ground-based observational window functions (von Braun et al. 2009). However, the Transiting Exoplanet Survey Satellite (TESS) has observed most of the sky during the primary mission (Ricker et al. 2015), including the known exoplanet hosts. The survey strategy of TESS thus provides a space-based means to systematically examine all of the known RV systems for potential transits of their planets that pass through inferior conjunction during the TESS observing window (Kane & von Braun 2008; Dalba et al. 2019). This has been demonstrated through the transit detection of an additional planet in the pi Mensae system (Huang et al. 2018) and the known RV planet in the HD 118203 system (Pepper et al. 2020).

HD 136352 (also known as Nu^2 Lupi, LHS 395, GJ 582, and HIP 75181) is a G-type main-sequence star that was observed for nearly 11 yr using the High Accuracy Radial velocity Planet Searcher (HARPS) spectrograph (Pepe et al. 2000). Analysis of the HARPS data by Udry et al. (2019) uncovered the signatures of three planets orbiting the star with periods and minimum masses in the range of 11–110 days and 5–10 $M_\oplus$, respectively. The host star was observed by TESS during Sector 12 of the primary mission. A TESS Guest Investigator (GI) program designed to monitor the known hosts (PI: Kane) immediately detected transits of the two inner planets (b and c). As of 2020 June 9, the HD 136352 system is one of less than 100 naked-eye exoplanet host stars in the sky, according to data from the NASA Exoplanet Archive (Akeson et al. 2013). HD 136352 is now also one of only three naked-eye stars that host more than one transiting planet, the other two systems being HD 219134 (Motalebi et al. 2015; Vogt et al. 2015; Gillon et al. 2017a) and HR 858 (Vanderburg et al. 2019). In all cases, the measurement accuracy correlates with the stellar magnitude, and therefore the search for transiting planets around bright stars is of paramount importance.

Here we present the detection of transits for the two inner planets of the HD 136352 system from TESS photometry, and we provide a combined analysis of all available RV and photometric data. In Section 2 we describe the transit probabilities of the planets and the properties of the host star. Section 3 provides details regarding the RV observations of the star and the detrending of the TESS photometry. A description of the data analysis is provided in Section 4, including a combined fit for all available data and a discussion of the location of the planets with respect to the overall demographics of exoplanets. In Section 5 we present a discussion of the potential for atmospheric characterization of the transiting planets. Suggestions for future work and concluding remarks are provided in Section 6.

2. System Properties

The HD 136352 system is known to host three planets with orbital periods of 11.6, 27.6, and 108.1 days. The planetary orbits are near-circular in nature, and the detailed properties of the new parameters provided by this work may be found in Section 4. Since the planets have short orbital periods, they also have relatively high geometric transit probabilities (Kane & von Braun 2008; Stevens & Gaudi 2013). We calculate the a priori transit probabilities as 4.88%, 2.77%, and 1.19% for the b, c, and d planets, respectively. A detailed analysis of transit probabilities for known RV exoplanets by Dalba et al. (2019) resulted in a prediction of about three transit detections during the TESS primary mission. Our reporting of transits for two of the HD 136352 planets, combined with the detected transit for HD 118203b (Pepper et al. 2020), brings the total number of RV planets revealed to be transiting in line with the Dalba et al. (2019) predictions. Note that the TESS extended mission will likely lead to further transit detections of known RV planets whose orbital periods are longer than TESS observations of their host star during the primary mission.

The host star HD 136352 is a G3/5V star that has been spectroscopically observed dozens of times over the last three decades (Hinkel et al. 2014). Compiling the observed stellar parameters, to be used as priors in Section 4.1, we found that the median stellar radius $R_* = 1.02 \pm 0.02\,R_\odot$, $T_{\rm eff} = 5692 \pm 218$ K, and $\log g = 4.39 \pm 0.33$, such that the

uncertainties reflect the *spread* or range in all of the measured values. The iron content, or [Fe/H], ranges from −0.16 dex (Carretta et al. 2000) to −0.46 dex (Francois 1986), with a median value of -0.29 ± 0.15 dex, where all observations were solar renormalized to Lodders et al. (2009). Based on the 32 other elemental abundances reported in the Hypatia Catalog (Hinkel et al. 2014), it is clear that HD 136352 is a relatively metal-poor star, consistent with the star's thick-disk kinematics. Some of the elements, particularly those in the iron peak and beyond the iron peak nucleosynthetic groups, have abundances that are more dramatically subsolar, such as $[Cr/H] = -0.31 \pm 0.14$ dex, $[Mn/H] = -0.48 \pm 0.25$ dex, and $[Y/H] = -0.34 \pm 0.07$ dex. On the other hand, the α-elements are closer to solar, such as $[O/H] = -0.02 \pm 0.15$ dex and $[Mg/H] = -0.04 \pm 0.15$ dex. The average of the α-elements, particularly C, O, Mg, Si, S, Ca, and Ti, is $[\alpha/H] = -0.12$ dex. The C/O molar fraction for HD 136352 is 0.35, where stars with a C/O ratio ∼0.8–1.0 are likely to produce geodynamically inactive planets (Bond et al. 2010; Unterborn et al. 2014; Hinkel & Unterborn 2018).

3. Observations

The observational data of the system considered here include almost 20 yr of precision RV measurements and one sector of TESS photometry during Cycle 1. The star is identified in the TESS Input Catalog (TIC) as TIC 136916387 (Stassun et al. 2018, 2019).

3.1. Radial Velocities

The RV data used for this analysis were acquired from three different observing facilities. The first data set consists of 246 RV measurements obtained over a period of 13.2 yr using the HARPS spectrograph, of which 240 measurements were previously published by Udry et al. (2019) when announcing the discovery of the HD 136352 system. The full details of the instrument and observations may be found in Udry et al. (2019) and references therein. Note that the most recent (six) HARPS measurements were acquired after an instrument upgrade and so were treated as an independent data set in the combined fit to the data described in Section 4.1. The second data set consists of 169 RV measurements obtained over a period of 17.3 yr using the UCLES high-resolution spectrograph (Diego et al. 1990) on the 3.9 m Anglo-Australian Telescope (AAT). The instrument uses an iodine absorption cell to provide wavelength calibration from 5000 to 6200 Å by embedding iodine absorption lines on the stellar spectrum (Valenti et al. 1995; Butler et al. 1996). The AAT RV observations were conducted as part of the Anglo-Australian Planet Search, described in more detail by Wittenmyer et al. (2020) and references therein. The third data set consists of 43 RV measurements obtained over a period of 12.0 yr using the HIRES echelle spectrograph on the Keck I telescope (Vogt et al. 1994), of which 23 measurements were previously published by Howard & Fulton (2016). The combined RV data set is shown in the top panel of Figure 1, and a subset of 10 RVs from each instrument is provided in Table 1. The mean measurement uncertainties are 0.42, 1.27, and 1.17 m s^{-1} for the HARPS, AAT, and HIRES data sets, respectively. Although the highest of these mean uncertainties is associated with the AAT data, the AAT data set also has the longest time baseline, making it a valuable addition to the analysis.

3.2. TESS Photometry

The TESS spacecraft observed HD 136352 during Sector 12 of its primary mission between 2019 May 21 and 2019 June 18. Because HD 136352 is a bright, nearby dwarf star, images from pixels surrounding the star were saved and downloaded every two minutes, compared to 30 minute sampling for most of the sky. These images were downlinked from the spacecraft, processed by the Science Processing Operations Center (SPOC) pipeline (based at NASA Ames Research Center), and searched for transits (Jenkins et al. 2016, 2020). The SPOC transiting-planet search algorithm detected a possible transit-like signal when it lined up one transit of HD 136352 b with the single transit of HD 136352 c, but the signal was rejected by an automated classification algorithm because the two transits have significantly different depths. HD 136352 was therefore not alerted as a TESS planet candidate host star. We subsequently identified the transits of HD 136352 b and c in a visual inspection of the light curve, which resulted in an allocated TESS Object of Interest number of 2011.

The light curve of HD 136352 produced by the SPOC pipeline contains residual systematic errors, so we extracted our own custom light curve from the TESS pixel data. Our approach is very similar to the one used by Vanderburg et al. (2019) to produce a light curve of another bright star, HR 858. We first extracted light curves of HD 136352 from 20 different photometric apertures. We then removed instrumental systematics by decorrelating each of the 20 light curves with other time series via matrix inversion (while excluding points in transit from the fit). In particular, we decorrelated against the first- and second-order time series of the means and standard deviations of the engineering quaternion measurements within each exposure. We also decorrelated against the high-frequency (band 3) common mode systematics in the cotrending basis vectors calculated by the SPOC Pre-search Data Conditioning module and the time series of background flux measurements (Smith et al. 2012; Stumpe et al. 2012, 2014). In total, we fit a model with 46 free parameters to the 16,865 out-of-transit data points. Finally, we calculated the point-to-point photometric scatter for each of the 20 light curves and chose the one with the highest precision. This procedure is described in more detail in Section 2.1 of Vanderburg et al. (2019).

The resulting decorrelated light curve still showed low-frequency variability (likely a combination of both slow instrumental drifts and astrophysical variability). We modeled these low-frequency trends with a basis spline and simultaneously determined the spline function along with the transit model parameters. We introduced discontinuities to the basis spline at the times of spacecraft momentum dumps. We removed the variability by dividing the best-fit spline from the light curve. Note that the amplitude of the low-frequency variability is less than a few hundred parts per million with timescales greater than 1 day. Though the variability amplitude is a large fraction of the transit depths described in Section 4, the timescales of the transits are much shorter, and we were thus able to effectively remove the variability with negligible effect on the subsequent data analysis. The light curve resulting from our detrending, with both instrumental systematics and stellar variability removed, is shown in Figure 1.

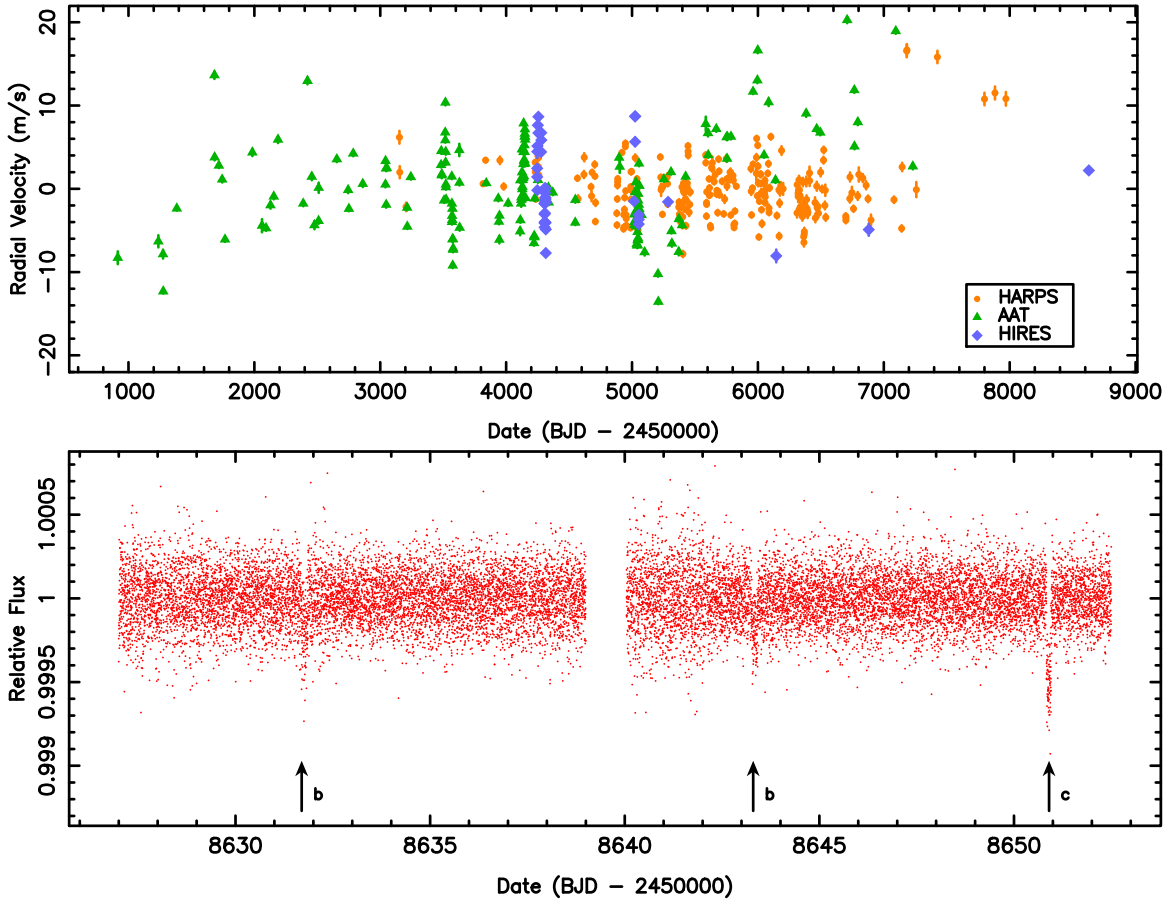

Figure 1. Primary data sources used in this analysis. Top: combined RV data spanning a period of 21 yr, acquired using the HARPS (orange circles), AAT/UCLES (green triangles), and Keck/HIRES (blue diamonds) instruments. Bottom: Sector 12 TESS photometry, with vertical arrows indicating the location of the two transits for planet b and the single transit for planet c.

4. Data Analysis

Here, we describe the extracted properties of the star and planets, as well as their location within the context of the known exoplanet population.

4.1. Extraction of System Parameters

Using the data described in Section 3, we performed our analysis using the EXOFASTV2 tool,[36] described in detail by Eastman et al. (2013, 2019). Following previous applications of EXOFASTV2 (e.g., Dalba et al. 2020), we conducted two fits to extract the system parameters. In the first, we fit archival photometry of HD 136352 to modeled spectral energy distributions (SEDs). We applied normal priors on the parameters $R_\star$, $M_\star$, $T_{\rm eff}$, and [Fe/H] using the values provided in Section 2. We also included a normal prior on parallax (68.164 ± 0.097 mas) based on measurements from the second data release of the Gaia mission (Gaia Collaboration et al. 2018) corrected for the systematic offset discovered by Stassun & Torres (2018). Lastly, we included an upper limit on the maximum line-of-sight extinction from the reddening maps from Schlafly & Finkbeiner (2011). This initial, SED-only fit converged upon the following stellar parameters: $R_\star = 1.010 \pm 0.018\,R_\odot$, $M_\star = 0.923 \pm 0.077\,M_\odot$, $T_{\rm eff} = 5851 \pm 110$ K, and [Fe/H] $= -0.25 \pm 0.14$ dex. These parameters were then used as priors for a global fit to the transit and RV data. We assessed convergence using the default EXOFASTV2 statistics of T_z (Ford 2006), the number of independent draws of the underlying posterior probability distribution (convergence for $T_z > 1000$ for each parameter), and GR, the well-known Gelman–Rubin statistic (Gelman & Rubin 1992), where convergence is achieved for GR < 1.01 for each parameter. The derived stellar parameters from this global fit are provided in Table 2. The planetary parameters are provided in Table 3. The zeroth-order RV offsets found by the fit were -68709.038 ± 0.094, -68697.2 ± 3.0, 0.17 ± 0.38, and -0.65 ± 0.64 m s^{-1} for the preupgrade HARPS, postupgrade HARPS, AAT, and HIRES data sets, respectively. The best-fit transit and RV models are shown in Figures 2 and 3.

Although transits of planets b and c were detected in the TESS photometry, we found no evidence of a transit for planet d. The question then is: do the photometric data rule out a transit for planet d, or did the planet not pass through inferior conjunction during the TESS observing window? Using the derived orbital properties of planet d from Table 3, we found that the nearest predicted inferior conjunction time occurs ~21 days prior to the commencement of Sector 12 observations. Thus, planet d may yet be found to also transit the host star with further observations. The inclinations of planets b and c are such that a perfectly coplanar planet d would not be transiting, but even a tiny mutual inclination of ~0°.3 would allow for a transit. In fact, planet d would only be transiting for inclinations between 90° and 89°.4, including grazing configurations, while assuming planet d has a radius similar to planet

[36] https://github.com/jdeast/EXOFASTv2

Table 1
HD 136352 RVs

Instrument	Date (BJD—2450000)	RV ($m\,s^{-1}$)	σ ($m\,s^{-1}$)
HARPS	3152.7661	6.188	0.770
HARPS	3154.6851	1.984	0.730
HARPS	3204.5378	−2.172	0.520
HARPS	3816.8345	0.609	0.280
HARPS	3836.7974	3.438	0.270
HARPS	3950.5459	3.422	0.460
HARPS	3980.4880	0.281	0.380
HARPS	4230.8179	3.180	0.300
HARPS	4231.7510	2.023	0.360
HARPS	4234.7314	−1.242	0.300
AAT	915.1653	−8.280	1.800
AAT	1237.2321	−6.310	3.380
AAT	1274.2877	−7.850	2.470
AAT	1276.1555	−12.310	3.210
AAT	1384.0170	−2.360	1.840
AAT	1683.0382	13.650	2.100
AAT	1684.1084	3.790	2.000
AAT	1718.0880	2.790	2.100
AAT	1743.9812	1.120	1.840
AAT	1766.8840	−6.080	2.040
HIRES	6145.7617	−8.060	1.288
HIRES	6880.7524	−4.906	1.400
HIRES	5024.8408	5.643	1.286
HIRES	5024.8418	8.699	1.252
HIRES	5024.8428	8.706	1.286
HIRES	5052.8169	−3.129	1.219
HIRES	5052.8184	−4.245	1.199
HIRES	5052.8198	−3.695	1.236
HIRES	4246.9380	1.427	1.239
HIRES	4246.9390	2.457	1.268

(This table is available in its entirety in machine-readable form.)

Table 2
HD 136352 Derived Stellar Parameters

Parameter	Units	Values
M_*	Mass ($M_\odot$)	$0.906^{+0.055}_{-0.047}$
R_*	Radius ($R_\odot$)	1.012 ± 0.018
L_*	Luminosity ($L_\odot$)	$1.081^{+0.088}_{-0.082}$
ρ_*	Density (cgs)	$1.234^{+0.098}_{-0.086}$
$\log g$	Surface gravity (cgs)	$4.385^{+0.029}_{-0.027}$
$T_{\rm eff}$	Effective temperature (K)	5850 ± 100
[Fe/H]	Proxy for metallicity (dex)	-0.25 ± 0.12
$[{\rm Fe/H}]_0$	Proxy for initial metallicity	-0.18 ± 0.11
Age	Age (Gyr)	$8.2^{+3.2}_{-3.1}$
A_V	V-band extinction (mag)	$0.060^{+0.071}_{-0.043}$
$\sigma_{\rm SED}$	SED photometry error scaling	$4.3^{+1.9}_{-1.1}$
ϖ	Parallax (mas)	68.159 ± 0.098
d	Distance (pc)	14.672 ± 0.021
Wavelength Parameters:		TESS
u_1	Linear limb-darkening coefficient	$0.275^{+0.039}_{-0.038}$
u_2	Quadratic limb-darkening coefficient	0.285 ± 0.035

c. Even so, conditioned on the fact that b and c transit, the probability that d transits is about 20% for typical mutual inclinations of $\sim 1°$.

4.2. Exoplanet Demographics

In Figure 4 (left panel), we show a mass–radius diagram that contains known exoplanets with measured masses (i.e., not $M \sin i$) and radii with uncertainties less than 15%. Figure 4 also includes modeled planetary composition models for rocky planets with or without H_2 envelopes from Zeng et al. (2019). Our data analyses from Section 4.1 show that the inner planet of HD 136352 is relatively small, with a radius of 1.482 $R_\oplus$. This, when compared with the mass of 4.62 $M_\oplus$, yields a bulk density of $7.8^{+1.2}_{-1.1}$ g cm^{-3} (see Table 3). A comparison to the 5.5 g cm^{-3} bulk density of Earth suggests that planet b has a dense core that is potentially iron dominated. Indeed, the planet b density lies near the peak density for rocky planets based on the empirical predictions of Weiss & Marcy (2014). Planet c, on the other hand, has a significantly larger radius of 2.608 $R_\oplus$, yielding a density of only $3.50^{+0.41}_{-0.36}$ g cm^{-3}, which is consistent with a thick hydrogen–helium envelope. This can be explained through the photoevaporation hypothesis that produces the radius valley in the exoplanet distribution (Lopez & Fortney 2013; Owen & Wu 2013; Fulton et al. 2017). According to this hypothesis, planet b would consist of a "bare" core, which, due to the proximity to the host star, would have suffered atmospheric stripping within 100 Myr of formation. HD 136352c, on the other hand, received less high-energy radiation and maintained a thick atmospheric envelope. Given the mass and radius for both planets, there are significant constraints for inferences to their interior structures in the context of composition. Namely, the stellar elemental abundances (see Section 2) would need to be measured to a higher precision, 0.02–0.04 dex (Hinkel & Unterborn 2018), necessary to meaningfully constrain the mineralogy (Unterborn & Panero 2019). In addition, fundamental to all of the mass–radius models are critical assumptions regarding the composition of rocky exoplanets and the underlying mineral physics. These assumptions typically cause over- or underpredictions in empirical models (e.g., Zeng et al. 2016) when characterizing ultrahigh pressures present in the cores of super-Earths and mini-Neptunes (Unterborn & Panero 2019).

To explore the evaporation hypothesis further, we produced the radius–insolation diagram shown in Figure 4 (right panel), including the planet radius versus stellar irradiation relative to the Earth ($S_\oplus$) for a sample of well-characterized confirmed exoplanets. Starting from all confirmed exoplanets listed on the NASA Exoplanet Archive,[37] we excluded those with a controversial flag, those with only a limit for planet radius, and those with planetary radii with errors greater than 15%. For the remaining planets, we either used the value of $S_\oplus$ provided or we calculated this value using the available stellar and orbital properties. This well-characterized sample cleanly displays a gap in the planetary radius distribution (e.g., Fulton et al. 2017). Interestingly, the inner transiting planets orbiting HD 136352 straddle this gap despite differing in stellar irradiation by only a factor of three (at the present time). This bifurcation in planet properties makes the HD 136352 system an excellent laboratory for testing the cause of the radius gap for small planets. Indeed, the two planets tend to have approximately the planetary radii suggested by the aforementioned evaporation model by Owen & Wu (2013): $1.3R_\oplus$ for a "stripped" core and $2.6R_\oplus$ for a mini-Neptune.

With the host star being similar to the Sun, the known HD 136352 planets lie far interior to the inner boundaries of

[37] https://exoplanetarchive.ipac.caltech.edu/

Table 3
HD 136352 Planetary Parameters

Parameter	Units	Values		
		b	c	d
P	Period (days)	$11.57779^{+0.00091}_{-0.0011}$	$27.5909^{+0.0028}_{-0.0031}$	$107.63^{+0.18}_{-0.19}$
R_p	Radius ($R_\oplus$)	$1.482^{+0.058}_{-0.056}$	$2.608^{+0.078}_{-0.077}$	…
M_p	Mass ($M_\oplus$)	$4.62^{+0.45}_{-0.44}$	$11.29^{+0.73}_{-0.69}$	…
T_C	Time of conjunction (BJD_{TDB})	$2458631.7672^{+0.0023}_{-0.0022}$	$2458650.8947^{+0.0011}_{-0.0010}$	$2458593.7^{+5.6}_{-5.5}$
T_0	Optimal conjunction time (BJD_{TDB})	$2458631.7672^{+0.0023}_{-0.0022}$	$2458650.8947^{+0.0011}_{-0.0010}$	$2455902.7^{+3.4}_{-2.7}$
a	Semimajor axis (au)	$0.0969^{+0.0019}_{-0.0017}$	$0.1729^{+0.0034}_{-0.0030}$	$0.4285^{+0.0085}_{-0.0076}$
i	Inclination (degrees)	$88.86^{+0.54}_{-0.30}$	$88.658^{+0.055}_{-0.057}$	…
e	Eccentricity	$0.079^{+0.068}_{-0.053}$	$0.037^{+0.039}_{-0.026}$	$0.075^{+0.085}_{-0.053}$
ω_*	Argument of periastron (degrees)	172^{+63}_{-67}	142^{+86}_{-92}	-175^{+79}_{-87}
T_{eq}	Equilibrium temperature (K)	911 ± 18	682^{+14}_{-13}	$433.3^{+8.6}_{-8.5}$
K	RV semiamplitude ($m\ s^{-1}$)	1.40 ± 0.13	2.55 ± 0.13	1.51 ± 0.14
R_p/R_*	Radius of planet in stellar radii	$0.01343^{+0.00044}_{-0.00045}$	0.02363 ± 0.00052	…
a/R_*	Semimajor axis in stellar radii	$20.60^{+0.53}_{-0.49}$	$36.76^{+0.95}_{-0.87}$	$91.1^{+2.3}_{-2.2}$
δ	Transit depth (fraction)	0.000180 ± 0.000012	$0.000558^{+0.000025}_{-0.000024}$	…
Depth	Flux decrement at midtransit	0.000180 ± 0.000012	$0.000558^{+0.000025}_{-0.000024}$	…
τ	Ingress/egress transit duration (days)	$0.00260^{+0.00043}_{-0.00033}$	0.0108 ± 0.0011	…
T_{14}	Total transit duration (days)	$0.1640^{+0.0048}_{-0.0045}$	$0.1337^{+0.0024}_{-0.0022}$	…
T_{FWHM}	FWHM transit duration (days)	$0.1613^{+0.0049}_{-0.0046}$	$0.1229^{+0.0023}_{-0.0022}$	…
b	Transit impact parameter	$0.41^{+0.12}_{-0.20}$	$0.854^{+0.013}_{-0.016}$	…
b_S	Eclipse impact parameter	$0.408^{+0.077}_{-0.18}$	$0.863^{+0.056}_{-0.040}$	…
τ_S	Ingress/egress eclipse duration (days)	$0.00261^{+0.00021}_{-0.00020}$	$0.0113^{+0.0035}_{-0.0017}$	…
$T_{S,14}$	Total eclipse duration (days)	$0.166^{+0.018}_{-0.014}$	$0.1321^{+0.0097}_{-0.020}$	…
$T_{S,FWHM}$	FWHM eclipse duration (days)	$0.163^{+0.018}_{-0.014}$	$0.121^{+0.011}_{-0.024}$	…
ρ_p	Density (cgs)	$7.8^{+1.2}_{-1.1}$	$3.50^{+0.41}_{-0.36}$	…
$\log g_p$	Surface gravity	$3.313^{+0.053}_{-0.054}$	$3.211^{+0.038}_{-0.037}$	…
Θ	Safronov number	$0.0234^{+0.0023}_{-0.0022}$	$0.0581^{+0.0035}_{-0.0034}$	…
$\langle F \rangle$	Incident flux (10^9 erg s^{-1} cm^{-2})	$0.155^{+0.013}_{-0.012}$	$0.0490^{+0.0040}_{-0.0038}$	$0.00790^{+0.00066}_{-0.00062}$
T_P	Time of periastron (BJD_{TDB})	$2458622.4^{+2.1}_{-1.9}$	2458626.9 ± 6.6	2458510^{+24}_{-25}
T_S	Time of eclipse (BJD_{TDB})	$2458625.63^{+0.37}_{-0.57}$	$2458636.93^{+0.39}_{-0.67}$	$2458536.8^{+6.6}_{-7.2}$
$e \cos \omega_*$	…	$-0.047^{+0.050}_{-0.077}$	$-0.010^{+0.022}_{-0.038}$	$-0.030^{+0.049}_{-0.10}$
$e \sin \omega_*$	…	$0.003^{+0.056}_{-0.057}$	$0.004^{+0.040}_{-0.027}$	$-0.002^{+0.050}_{-0.058}$
$M_p \sin i$	Minimum mass ($M_\oplus$)	$4.62^{+0.45}_{-0.43}$	$11.28^{+0.73}_{-0.69}$	$10.5^{+1.1}_{-1.0}$
M_p/M_*	Mass ratio	0.0000153 ± 0.0000014	0.0000373 ± 0.0000021	$0.0000346^{+0.0000033}_{-0.0000032}$
d/R_*	Separation at midtransit	20.4 ± 1.3	$36.5^{+1.5}_{-1.6}$	$90.9^{+5.5}_{-5.7}$

the Habitable Zone (Kasting et al. 1993; Kopparapu et al. 2013, 2014; Kane et al. 2016a), but they do lie within the Venus Zone (Kane et al. 2014). This is mostly relevant to planet b and other terrestrial planets that may be present within the system, because the exploration of planetary habitability and comparative planetology aims to study the major factors that drive the bifurcation of habitable versus uninhabitable environments (Hamano et al. 2013; Kane et al. 2019; Way & Del Genio 2020). Terrestrial planets orbiting close to a bright host star, such as those discussed here, provide the best opportunities to conduct the needed atmospheric studies to inform the diversification processes (Ostberg & Kane 2019).

5. Atmospheric Characterization

In order to quantify the expected follow-up potential to observe the atmospheres of HD 136352 b and c, we calculated their estimated transmission spectroscopy signal-to-noise ratios (S/N) using the transmission spectroscopy metric (TSM) developed by Kempton et al. (2018). This metric is dependent on the planet radius, mass, and equilibrium temperature, as well as the stellar radius and apparent J-band magnitude. The TSM method also includes a scale factor that is dependent on the radius of the planet that allows the TSM values to have a 1:1 ratio with simulated Near Infrared Slitless Spectrograph (NIRISS) results produced by Louie et al. (2018), which assumes 10 hr of observations with NIRISS on board the James Webb Space Telescope (JWST). By applying the values for both of the HD 136352 transiting planets obtained through Tables 2 and 3, we find that the estimated TSM values for the b and c planets are 12 and 148, respectively.

To provide context for the estimated atmospheric observability of HD 136352b and c, we compared their TSM values to those of the TRAPPIST-1 planets. Using the stellar and planetary parameters from Gillon et al. (2017b), we calculated the TSM values for TRAPPIST-1b–g to be 44, 21, 24, 23, 27, and 15, respectively. This illustrates that HD 136352b would be expected to require more observation time to achieve the same S/N as the TRAPPIST-1 planets, while HD 136352c would require far less time. The stark difference in estimated S/N between the HD 136352 planets is due to their differences in planetary radii and the expected compositions of their atmospheres. Since the TSM calculation is proportional to the planetary radius to the third

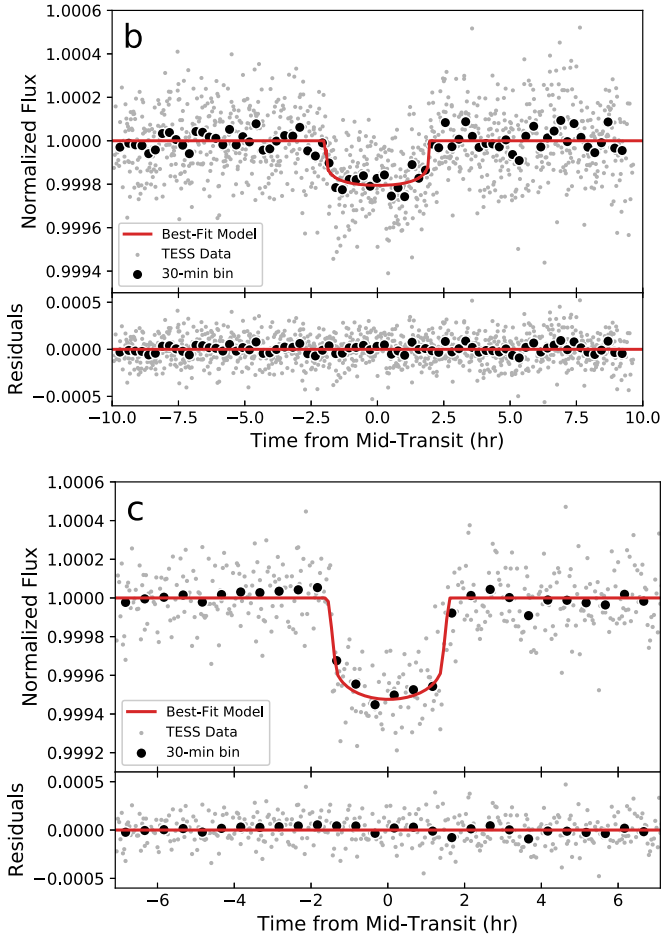

Figure 2. Transit fits to the TESS photometry resulting from the EXOFAST analysis, described in Section 4.1. Top: transit of the b planet where both transits have been folded on the orbital period of the planet. Bottom: single transit of the c planet.

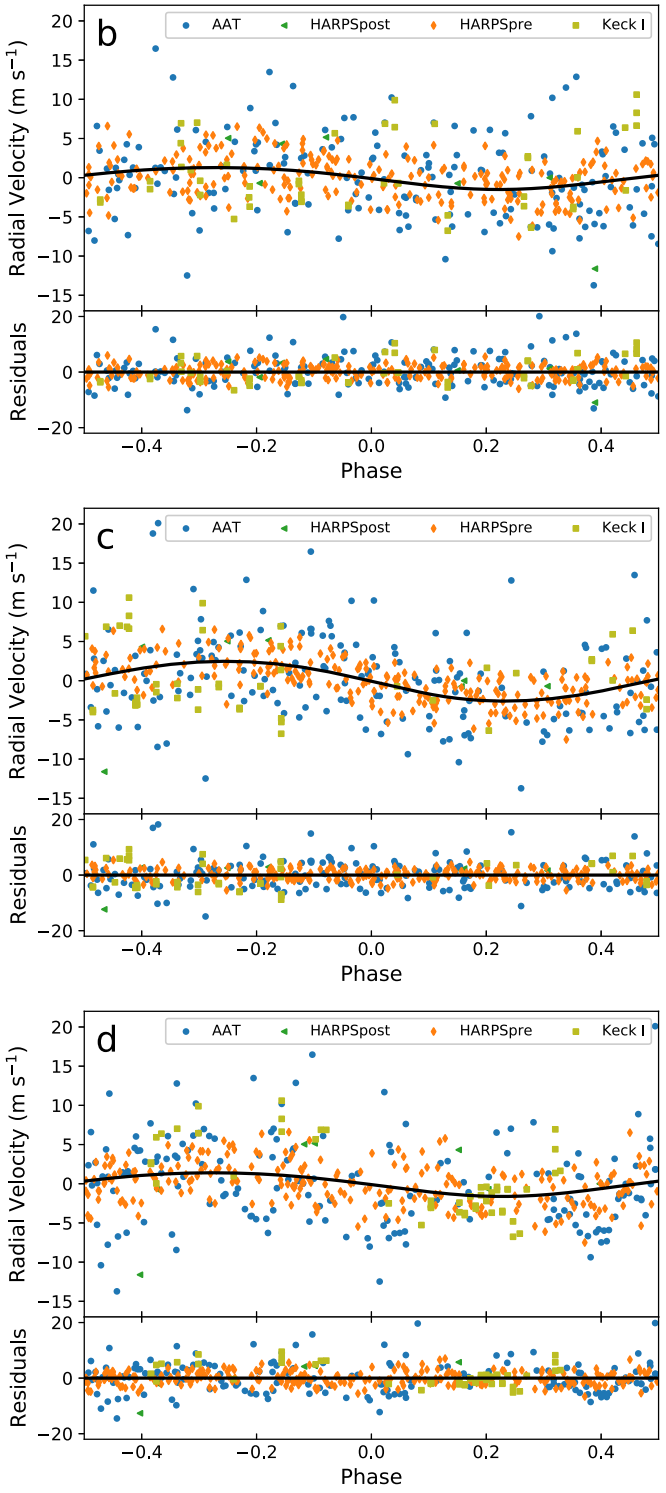

Figure 3. Combined RV data set after applying the EXOFAST fits described in Section 4.1. The RV data are folded on the orbital period for each planet, including the b (top), c (middle), and d (bottom) planets.

power, the larger radius of HD 136352c gives it a steep increase in estimated S/N. Furthermore, HD 136352b is not expected to have a hydrogen-dominated atmosphere, and thus the original simulations of Louie et al. (2018) assume a mean molecular weight that is nearly 10 times larger for this type of planet than for planets like HD 136352c ($\mu = 18$ versus 2.3). This leads to a correspondingly smaller S/N, due to the inverse linear dependence of transmission spectrum feature sizes on atmospheric mean molecular weight (Miller-Ricci et al. 2009). Even so, prospects exist for potential detection of an extended atmosphere for HD 136352c, through mechanisms such as helium absorption (Allart et al. 2018).

It should be noted that HD 136352's *K*-band magnitude of 4.159 may result in observations by JWST being difficult because the saturation limit for spectroscopy is $K \sim 4$ (Beichman et al. 2014). Therefore, ground-based, high-resolution transmission spectroscopy using the cross-correlation method (Snellen et al. 2010) may be a more productive avenue to pursue because this technique is ideally suited to planets orbiting very bright host stars. The TSM values we calculated should also be proportional to the S/N expected in the near-infrared with this technique.

6. Conclusions

RV exoplanet systems are among the best-characterized systems in the overall exoplanet inventory. This is because the brightness of the host stars enables significant observational capability and ancillary science, including the study of planetary orbits, architectures, and interactions (Ford 2014; Kane & Raymond 2014; Winn & Fabrycky 2015). The ancillary science includes investigations of the radius gap, evaporation scenarios, and the structure of planets that span the planetary radius gap (Mousis et al. 2020). Furthermore, the

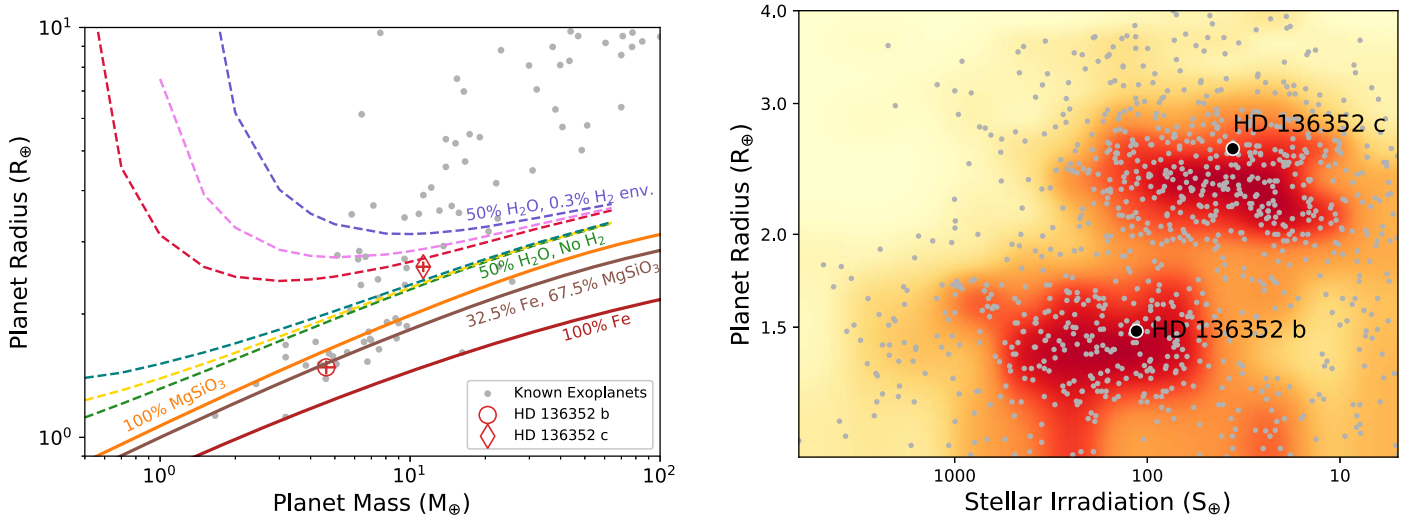

Figure 4. Location of the HD 136352 b and c planets with respect to exoplanet demographic populations. Left: mass–radius diagram including known planets with mass and radius uncertainties less than 15%. The locations of the b and c planets are marked as indicated. Also shown are models for planets of various compositions with or without H_2 envelopes (Zeng et al. 2019). Right: planet radius and stellar irradiation for a sample of well-characterized confirmed exoplanets (gray points) with better than 15% precision in the measured radius value. The background colors describe the density of data points, with darker tones having more points. The inner transiting planets orbiting HD 136352 exist on opposite sides of the small planet radius gap.

relative proximity of the RV systems makes them attractive targets for direct imaging surveys that aim to directly detect the known planets (Kane 2013; Kane et al. 2018; Kopparapu et al. 2018). Thus, when planets in RV systems are also found to transit their host star, they become truly exceptional in the scope of possible science, particularly when multiple planets are found to transit in the same system.

The trajectory of exoplanetary science is leading toward the characterization of planetary atmospheres. In order to fully exploit the potential of transmission spectroscopy techniques, numerous excellent targets are required that orbit bright host stars. The HD 136352 system is now known to harbor two transiting planets, and our analysis has determined that the radii of these planets place them on either side of the well-known radius gap. As described in Section 5, the imperative to understand the atmospheric evolution of such planets makes them attractive follow-up targets for atmospheric studies. We have shown that planet c is an especially promising target in terms of the expected S/N from both transmission and emission spectroscopy observations that could be carried out with JWST.

One pressing concern is that, despite long-term constraints from RVs and from the single transit, the period of planet c is still relatively uncertain. Therefore, further observations, either during the TESS extended mission or by the CHEOPS mission (Broeg et al. 2014), are needed to ensure that the ephemeris of this planet can be refined to enable followed-up observations (Dragomir et al. 2020). As noted in Section 4.1, planet d did not pass through inferior conjunction during the TESS observations, so follow-up photometric campaigns could reveal whether planet d also transits.

As described in Section 1, the transit detection of known RV planets has historically provided some of the most interesting exoplanets over the past two decades. This work demonstrates that this is still true, and the advantage of RV observations has enabled us to provide significant mass constraints, due to the legacy of RV observations that preceded the transit detections. With the TESS mission transitioning into a mode whereby it returns to previously observed parts of the sky, we can expect that there will be further opportunities to uncover new insights into the known exoplanetary systems.

The authors would like to thank Jason Eastman for helpful instruction regarding the use of EXOFASTV2, and the anonymous referee whose feedback improved the manuscript. S.R.K. acknowledges support by the National Aeronautics and Space Administration through the TESS Guest Investigator Program (17-TESS17C-1-0004). P.D. acknowledges support from a National Science Foundation Astronomy and Astrophysics Postdoctoral Fellowship under award AST-1903811. S. U., F.B., X.D., D.E, C.L., F.P., M.M., and D.S. acknowledge the financial support of the National Center for Competence in Research, PlanetS, of the Swiss National Science Foundation (SNSF). D.E. acknowledges support from the European Research Council (ERC) under the European Unions Horizon 2020 research and innovation program (project FOUR ACES; grant agreement No. 724427). T.L.C. acknowledges support from the European Union's Horizon 2020 research and innovation program under the Marie Skłodowska-Curie grant agreement No. 792848 (PULSATION). H.R.A.J. is supported by UK STFC grant ST/R006598/1. We acknowledge the traditional owners of the land on which the AAT stands, the Gamilaraay people, and pay our respects to elders past and present. We gratefully acknowledge the efforts and dedication of the Keck Observatory staff for support of HIRES and remote observing. We recognize and acknowledge the cultural role and reverence that the summit of Maunakea has within the indigenous Hawaiian community. We are deeply grateful to have the opportunity to conduct observations from this mountain. Funding for the TESS mission is provided by NASA's Science Mission directorate. This research has made use of the Exoplanet Follow-up Observation Program website, which is operated by the California Institute of Technology, under contract with the National Aeronautics and Space Administration under the Exoplanet Exploration Program. Resources supporting this work were provided by the NASA High-End Computing (HEC) Program through the NASA Advanced Supercomputing (NAS) Division at Ames Research

Center for the production of the SPOC data products. This paper includes data collected by the TESS mission, which are publicly available from the Mikulski Archive for Space Telescopes (MAST). The research shown here acknowledges use of the Hypatia Catalog Database, an online compilation of stellar abundance data as described in Hinkel et al. (2014), which was supported by NASA's Nexus for Exoplanet System Science (NExSS) research coordination network and the Vanderbilt Initiative in Data-Intensive Astrophysics (VIDA). This research has made use of the NASA Exoplanet Archive, which is operated by the California Institute of Technology, under contract with the National Aeronautics and Space Administration under the Exoplanet Exploration Program. The results reported herein benefited from collaborations and/or information exchange within NASA's Nexus for Exoplanet System Science (NExSS) research coordination network sponsored by NASA's Science Mission Directorate.

Software: EXOFAST (Eastman et al. 2013, 2019).

ORCID iDs

Stephen R. Kane https://orcid.org/0000-0002-7084-0529
Selçuk Yalçınkaya https://orcid.org/0000-0002-5224-247X
Hugh P. Osborn https://orcid.org/0000-0002-4047-4724
Paul A. Dalba https://orcid.org/0000-0002-4297-5506
Louise D. Nielsen https://orcid.org/0000-0002-0091-9362
Andrew Vanderburg https://orcid.org/0000-0001-7246-5438
Teo Močnik https://orcid.org/0000-0003-4603-556X
Natalie R. Hinkel https://orcid.org/0000-0003-0595-5132
Colby Ostberg https://orcid.org/0000-0001-7968-0309
Ekrem Murat Esmer https://orcid.org/0000-0002-6191-459X
Stéphane Udry https://orcid.org/0000-0001-7576-6236
Tara Fetherolf https://orcid.org/0000-0002-3551-279X
Özgür Baştürk https://orcid.org/0000-0002-4746-0181
George R. Ricker https://orcid.org/0000-0003-2058-6662
Roland Vanderspek https://orcid.org/0000-0001-6763-6562
David W. Latham https://orcid.org/0000-0001-9911-7388
Sara Seager https://orcid.org/0000-0002-6892-6948
Joshua N. Winn https://orcid.org/0000-0002-4265-047X
Jon M. Jenkins https://orcid.org/0000-0002-4715-9460
Romain Allart https://orcid.org/0000-0002-1199-9759
Jeremy Bailey https://orcid.org/0000-0002-5726-7000
Jacob L. Bean https://orcid.org/0000-0003-4733-6532
Francois Bouchy https://orcid.org/0000-0002-7613-393X
R. Paul Butler https://orcid.org/0000-0003-1305-3761
Tiago L. Campante https://orcid.org/0000-0002-4588-5389
Brad D. Carter https://orcid.org/0000-0003-0035-8769
Tansu Daylan https://orcid.org/0000-0002-6939-9211
Magali Deleuil https://orcid.org/0000-0001-6036-0225
Rodrigo F. Diaz https://orcid.org/0000-0001-9289-5160
Xavier Dumusque https://orcid.org/0000-0002-9332-2011
David Ehrenreich https://orcid.org/0000-0001-9704-5405
Jonathan Horner https://orcid.org/0000-0002-1160-7970
Andrew W. Howard https://orcid.org/0000-0001-8638-0320
Howard Isaacson https://orcid.org/0000-0002-0531-1073
Hugh R. A. Jones https://orcid.org/0000-0003-0433-3665
Martti H. Kristiansen https://orcid.org/0000-0002-2607-138X
Christophe Lovis https://orcid.org/0000-0001-7120-5837
Geoffrey W. Marcy https://orcid.org/0000-0002-2909-0113
Maxime Marmier https://orcid.org/0000-0001-5630-1396
Simon J. O'Toole https://orcid.org/0000-0003-2839-8527
Darin Ragozzine https://orcid.org/0000-0003-1080-9770
Damien Ségransan https://orcid.org/0000-0003-2355-8034
C. G. Tinney https://orcid.org/0000-0002-7595-0970
Margaret C. Turnbull https://orcid.org/0000-0002-0569-1643
Robert A. Wittenmyer https://orcid.org/0000-0001-9957-9304
Duncan J. Wright https://orcid.org/0000-0001-7294-5386
Jason T. Wright https://orcid.org/0000-0001-6160-5888

References

Akeson, R. L., Chen, X., Ciardi, D., et al. 2013, PASP, 125, 989
Allart, R., Bourrier, V., Lovis, C., et al. 2018, Sci, 362, 1384
Beichman, C., Benneke, B., Knutson, H., et al. 2014, PASP, 126, 1134
Bond, J. C., Lauretta, D. S., & O'Brien, D. P. 2010, Icar, 205, 321
Bouchy, F., Udry, S., Mayor, M., et al. 2005, A&A, 444, L15
Broeg, C., Benz, W., Thomas, N. & Cheops Team 2014, CoSka, 43, 498
Butler, R. P., Marcy, G. W., Williams, E., et al. 1996, PASP, 108, 500
Carretta, E., Gratton, R. G., & Sneden, C. 2000, A&A, 356, 238
Charbonneau, D., Brown, T. M., Latham, D. W., & Mayor, M. 2000, ApJL, 529, L45
Dalba, P. A., Gupta, A. F., Rodriguez, J. E., et al. 2020, AJ, 159, 241
Dalba, P. A., Kane, S. R., Barclay, T., et al. 2019, PASP, 131, 034401
Diego, F., Charalambous, A., Fish, A. C., & Walker, D. D. 1990, Proc. SPIE, 1235, 562
Dragomir, D., Harris, M., Pepper, J., et al. 2020, AJ, 159, 219
Dragomir, D., Kane, S. R., Henry, G. W., et al. 2012, ApJ, 754, 37
Eastman, J., Gaudi, B. S., & Agol, E. 2013, PASP, 125, 83
Eastman, J. D., Rodriguez, J. E., Agol, E., et al. 2019, arXiv:1907.09480
Fabrycky, D. C., & Winn, J. N. 2009, ApJ, 696, 1230
Ford, E. B. 2006, ApJ, 642, 505
Ford, E. B. 2014, PNAS, 111, 12616
Fossey, S. J., Waldmann, I. P., & Kipping, D. M. 2009, MNRAS, 396, L16
Francois, P. 1986, A&A, 160, 264
Fulton, B. J., Petigura, E. A., Howard, A. W., et al. 2017, AJ, 154, 109
Gaia Collaboration, Brown, A. G. A., Vallenari, A., et al. 2018, A&A, 616, A1
Garcia-Melendo, E., & McCullough, P. R. 2009, ApJ, 698, 558
Gelman, A., & Rubin, D. B. 1992, StaSc, 7, 457
Gillon, M., Demory, B.-O., van Grootel, V., et al. 2017a, NatAs, 1, 0056
Gillon, M., Triaud, A. H. M. J., Demory, B.-O., et al. 2017b, Natur, 542, 456
Hamano, K., Abe, Y., & Genda, H. 2013, Natur, 497, 607
Henry, G. W., Kane, S. R., Wang, S. X., et al. 2013, ApJ, 768, 155
Henry, G. W., Marcy, G. W., Butler, R. P., & Vogt, S. S. 2000, ApJL, 529, L41
Hinkel, N. R., Kane, S. R., Pilyavsky, G., et al. 2015, AJ, 150, 169
Hinkel, N. R., Timmes, F. X., Young, P. A., Pagano, M. D., & Turnbull, M. C. 2014, AJ, 148, 54
Hinkel, N. R., & Unterborn, C. T. 2018, ApJ, 853, 83
Howard, A. W., & Fulton, B. J. 2016, PASP, 128, 114401
Huang, C. X., Burt, J., Vanderburg, A., et al. 2018, ApJL, 868, L39
Jenkins, J. M., Tenenbaum, P., Seader, S., et al. 2020, Kepler Data Processing Handbook: Transiting Planet Search, Kepler Data Processing Handbook KSCI-19081-003
Jenkins, J. M., Twicken, J. D., McCauliff, S., et al. 2016, Proc. SPIE, 9913, 99133E
Jontof-Hutter, D., Ford, E. B., Rowe, J. F., et al. 2016, ApJ, 820, 39
Kane, S. R. 2013, ApJ, 766, 10
Kane, S. R., Arney, G., Crisp, D., et al. 2019, JGRE, 124, 2015
Kane, S. R., Henry, G. W., Dragomir, D., et al. 2011a, ApJL, 735, L41
Kane, S. R., Hill, M. L., Kasting, J. F., et al. 2016a, ApJ, 830, 1
Kane, S. R., Howard, A. W., Pilyavsky, G., et al. 2011b, ApJ, 733, 28
Kane, S. R., Kopparapu, R. K., & Domagal-Goldman, S. D. 2014, ApJL, 794, L5
Kane, S. R., Mahadevan, S., von Braun, K., Laughlin, G., & Ciardi, D. R. 2009, PASP, 121, 1386
Kane, S. R., Meshkat, T., & Turnbull, M. C. 2018, AJ, 156, 267
Kane, S. R., & Raymond, S. N. 2014, ApJ, 784, 104
Kane, S. R., Thirumalachari, B., Henry, G. W., et al. 2016b, ApJL, 820, L5
Kane, S. R., & von Braun, K. 2008, ApJ, 689, 492
Kasting, J. F., Whitmire, D. P., & Reynolds, R. T. 1993, Icar, 101, 108
Kempton, E. M. R., Bean, J. L., Louie, D. R., et al. 2018, PASP, 130, 114401

Kopparapu, R. K., Hébrard, E., Belikov, R., et al. 2018, ApJ, 856, 122
Kopparapu, R. K., Ramirez, R., Kasting, J. F., et al. 2013, ApJ, 765, 131
Kopparapu, R. K., Ramirez, R. M., SchottelKotte, J., et al. 2014, ApJL, 787, L29
Kreidberg, L., Koll, D. D. B., Morley, C., et al. 2019, Natur, 573, 87
Laughlin, G., Deming, D., Langton, J., et al. 2009, Natur, 457, 562
Lodders, K., Palme, H., & Gail, H. P. 2009, LanB, 4B, 712
Lopez, E. D., & Fortney, J. J. 2013, ApJ, 776, 2
Louie, D. R., Deming, D., Albert, L., et al. 2018, PASP, 130, 044401
Miller-Ricci, E., Seager, S., & Sasselov, D. 2009, ApJ, 690, 1056
Motalebi, F., Udry, S., Gillon, M., et al. 2015, A&A, 584, A72
Mousis, O., Deleuil, M., Aguichine, A., et al. 2020, ApJL, 896, L22
Naef, D., Latham, D. W., Mayor, M., et al. 2001, A&A, 375, L27
Ostberg, C., & Kane, S. R. 2019, AJ, 158, 195
Owen, J. E., & Wu, Y. 2013, ApJ, 775, 105
Pepe, F., Mayor, M., Delabre, B., et al. 2000, Proc. SPIE, 4008, 582
Pepper, J., Kane, S. R., Rodriguez, J. E., et al. 2020, AJ, 159, 243
Pilyavsky, G., Mahadevan, S., Kane, S. R., et al. 2011, ApJ, 743, 162
Ricker, G. R., Winn, J. N., Vanderspek, R., et al. 2015, JATIS, 1, 014003
Schlafly, E. F., & Finkbeiner, D. P. 2011, ApJ, 737, 103
Sing, D. K., Fortney, J. J., Nikolov, N., et al. 2016, Natur, 529, 59
Smith, J. C., Stumpe, M. C., van Cleve, J. E., et al. 2012, PASP, 124, 1000
Snellen, I. A. G., de Kok, R. J., de Mooij, E. J. W., & Albrecht, S. 2010, Natur, 465, 1049
Stassun, K. G., Oelkers, R. J., Paegert, M., et al. 2019, AJ, 158, 138
Stassun, K. G., Oelkers, R. J., Pepper, J., et al. 2018, AJ, 156, 102
Stassun, K. G., & Torres, G. 2018, ApJ, 862, 61
Stevens, D. J., & Gaudi, B. S. 2013, PASP, 125, 933
Stumpe, M. C., Smith, J. C., Catanzarite, J. H., et al. 2014, PASP, 126, 100
Stumpe, M. C., Smith, J. C., van Cleve, J. E., et al. 2012, PASP, 124, 985
Udry, S., Dumusque, X., Lovis, C., et al. 2019, A&A, 622, A37
Unterborn, C. T., Kabbes, J. E., Pigott, J. S., Reaman, D. M., & Panero, W. R. 2014, ApJ, 793, 124
Unterborn, C. T., & Panero, W. R. 2019, JGRE, 124, 1704
Valenti, J. A., Butler, R. P., & Marcy, G. W. 1995, PASP, 107, 966
Vanderburg, A., Huang, C. X., Rodriguez, J. E., et al. 2019, ApJL, 881, L19
Vogt, S. S., Allen, S. L., Bigelow, B. C., et al. 1994, Proc. SPIE, 2198, 362
Vogt, S. S., Burt, J., Meschiari, S., et al. 2015, ApJ, 814, 12
von Braun, K., Kane, S. R., & Ciardi, D. R. 2009, ApJ, 702, 779
Wang, X. S., Wright, J. T., Cochran, W., et al. 2012, ApJ, 761, 46
Way, M. J., & Del Genio, A. D. 2020, JGRE, 125, e06276
Weiss, L. M., & Marcy, G. W. 2014, ApJL, 783, L6
Winn, J. N., & Fabrycky, D. C. 2015, ARA&A, 53, 409
Wittenmyer, R. A., Wang, S., Horner, J., et al. 2020, MNRAS, 492, 377
Zeng, L., Jacobsen, S. B., Sasselov, D. D., et al. 2019, PNAS, 116, 9723
Zeng, L., Sasselov, D. D., & Jacobsen, S. B. 2016, ApJ, 819, 127